Lithium surface-response modelling for the NSTX liquid lithium divertor

2011 Nucl. Fusion 51 023002

(http://iopscience.iop.org/0029-5515/51/2/023002)

IOP Publishing and International Atomic Energy Agency Nuclear Fusion
Nucl. Fusion **51** (2011) 023002 (8pp) doi:10.1088/0029-5515/51/2/023002

Lithium surface-response modelling for the NSTX liquid lithium divertor

J.P. Allain and J.N. Brooks

School of Nuclear Engineering, Purdue University, West Lafayette, Indiana 47907, USA

Received 20 September 2010, accepted for publication 21 December 2010
Published 25 January 2011
Online at stacks.iop.org/NF/51/023002

Abstract
We analyse lithium sputtering, evaporation and transport for the National Spherical Torus Experiment (NSTX) liquid lithium divertor (LLD) for planned high heating power plasma conditions. A temperature-dependent, data-calibrated, surface-response model is used to specify sputter yield, velocity distributions, sputtered Li ion fraction and related phenomena, for the static liquid lithium surface with D, Li and trace C impingement. Using the surface-response model, and supplied UEDGE code edge plasma parameters and LLD surface temperature profile for a typical 2 MW heating, low D-recycle shot, the REDEP/WBC code package computes Li erosion/redeposition. The results are encouraging showing negligible Li evaporation, moderate sputter erosion, and acceptable Li transport to the edge (∼7% Li/D density) and core plasma (∼1% Li/D contamination potential) and LLD adjacent surfaces. A 2% carbon plasma content does not significantly affect the LLD surface response. For fixed plasma conditions, but with hypothetically higher surface temperatures than the reference 281 °C peak, an increase to ∼350 °C appears acceptable, thus implying a significant operating temperature margin.

(Some figures in this article are in colour only in the electronic version)

1. Introduction

Lithium is being used to control particle and impurity control in tokamak and stellerator plasmas, e.g. [1–4]. The salient properties of lithium *conditioning* include low-recycling of hydrogen, ELM suppression and enhanced plasma performance [2]. Use of full *liquid lithium* has the added advantage of a high heat flux capable of replenishing plasma-facing surface. The Lithium Tokamak Experiment (LTX) will soon operate with thin films of liquid lithium, and the National Spherical Torus Experiment (NSTX) has recently introduced a full toroidal liquid lithium divertor (LLD) in a major tokamak.

A key issue for a lithium plasma-facing surface—in addition to MHD concerns—is evaporation and sputtering, both increasing with surface temperature, and resulting core-plasma content. Due to the high Li vapour pressure, there is a relatively low operating window ∼180–500 °C for liquid lithium operation. Another more subtle issue is whether the liquid lithium is static or flowing. In particular, static Li (and other liquid metals) is subject to surface mixing with impurities that could compromise the preferred properties of hydrogen retention and surface self-healing. The LLD surface in NSTX will be static and will comprise about 10% of the plasma-wetted area in NSTX. Therefore, since NSTX is a graphite machine, carbon impurity mixing on the LLD surface is a concern.

In a previous paper [5] an LLD forerunner design for NSTX was analysed by coupled codes/models for the plasma edge, divertor temperature, Li sputtering and erosion/redeposition. The D-pumping lithium surface yielded a low-recycle scrape-off layer (SOL) plasma with high plasma temperature and low density. Acceptable coating lifetime for a 2 s pulse and low core-plasma contamination by sputtered lithium was predicted.

In this work we extend surface-response models of liquid lithium with more sophisticated treatment of particle-induced absolute and differential sputtering, secondary sputtered ion fraction and evaporation. We examine four surface issues: sputter yields, C/Li mixing, sputtered Li charge state and low-energy Li reflection. This work is then applied to a typical RF heated plasma regime simulated by UEDGE [6] and coupled to the REDEP/WBC code package [7] to study erosion and transport of lithium particles in the LLD geometry of NSTX. We include time-dependent analysis of carbon–lithium mixing under carbon-seeded plasma conditions to predict lithium emission and transport.

As for the earlier NSTX analysis [5], the purpose of the REDEP analysis is to determine lithium surface erosion, lithium transport in the plasma and acceptability of the divertor surface temperature—as set by sputtering and evaporation. Key outputs are the Li/D ratio in the plasma near-surface region, and the core-plasma contamination potential. We also estimate the current of sputtered lithium from the LLD to adjacent carbon surfaces and the D-pumping capability of the resulting Li on C as well as the role of carbon impurities on the liquid Li surface and consequent operation of the LLD.

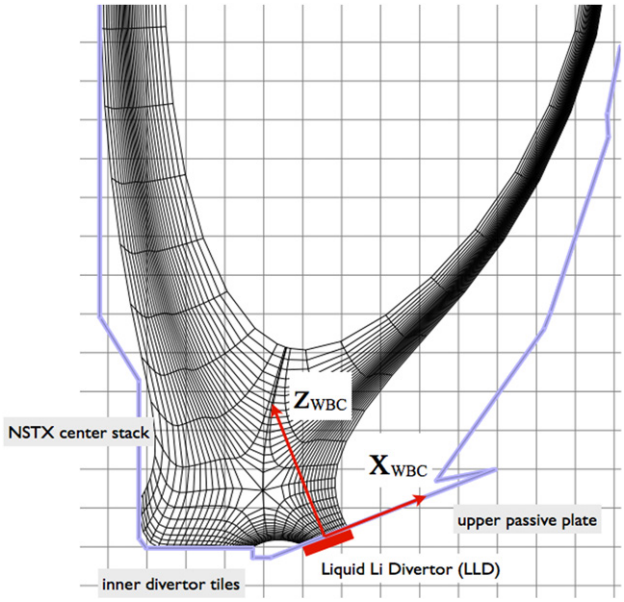

Figure 1. UEDGE NSTX computational grid (Stotler) superimposed on NSTX geometry. LLD is as shown.

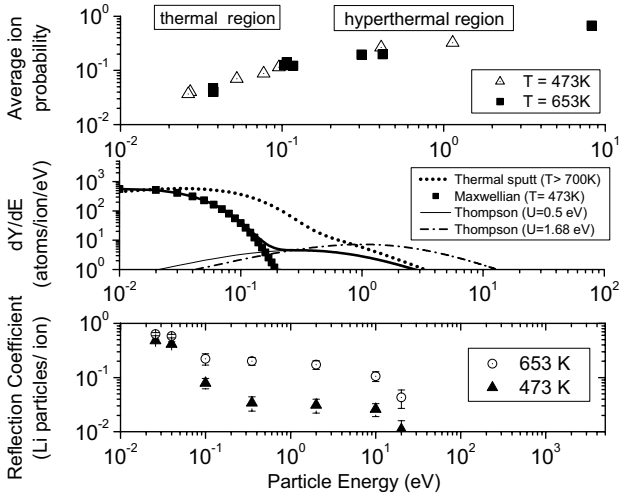

Figure 2. Temperature-dependent models of emitted (i.e. reflected, sputtered, etc) Li particles based on new atomistic model coupled with BCA-based ballistics. First frame shows average ion probability of emitted particles, second the temperature-dependent emitted particle energy distributions for temperature-dependent surface binding energies determined from MD-TRIM and last frame the Li reflection coefficient for two temperatures as a function of incident particle energy.

2. Liquid lithium divertor

NSTX is a low aspect ratio spherical torus ($R = 0.86$ m, $a = 0.67$ m) with neutral beam and RF heating. The goal of NSTX is to determine the attractiveness of the spherical torus concept, and to study plasma performance generally, in support of the overall tokamak mission including ITER. The LLD has emerged as a critical component for NSTX particle control, and to some extent for power handling, in support of the advanced physics mission including planned upgrades [2]. Figure 1 shows the NSTX geometry and LLD location. LLD consists of a full toroidal tray of molybdenum coated stainless steel on a thick copper substrate that will be filled with liquid lithium, and serve as most of the outer divertor target.

3. Liquid Li surface model

3.1. Temperature-dependent sputtering of D-containing lithium

Physical sputtering from liquid lithium has been studied extensively both in linear plasma devices and laboratory particle-beam experiments, e.g. [8, 9]. The sputter yield of lithium atoms can decrease by 40–45% when exposed to deuterium plasmas due to the dilution effect of deuterium at the lithium sputter depth. Incident deuterium particles with energies between 50 and 5 keV will implant in a projected range between approximately 5 and 200 nm into the lithium surface. Lithium melts at 180.5 °C and just above this melting point lithium sputtering does not vary much with temperature. At temperatures higher than 300–400 °C deuterium can diffuse readily, resulting in an effective pumping region that is about 250 nm deep. In contrast, particles sputtered by deuterium emanate from the first 2–3 surface monolayers. Recycling of implanted deuterium into the edge plasma is rate limited by recombination in the first monolayer. Therefore, the surface conditions (impurity implantation, deuterium coverage, water adsorption, etc) can have dramatic effects on surface erosion and recombination processes. The sputter rate of lithium atoms does not depend on the condensed matter phase (i.e. liquid versus solid) until about $T/T_m \sim 1.5$.

We compute liquid lithium sputtering yields here using the TRIM-SP code combined with a semi-empirical temperature-dependent model using experimental data by Allain *et al* [8]. The liquid Li surface model used in TRIM-SP assumes a temperature-dependent binding energy for surface atoms developed on the basis of atomistic simulations of lithium self-bombardment and D^+ bombardment as a function of temperature [10, 11]. Figure 2 shows the result of temperature-dependent Li particle emission based on the semi-empirical temperature-dependent models referenced above. In figure 2(*a*) the probability of a particle being emitted as a Li^+ ion is plotted as a function of emitted particle energy. Further discussion on the role of the ion probability in this analysis is included in section 3.3. Figure 2 also shows the sputtered energy distribution of particles as a function of surface temperature. A Maxwellian distribution is used to model for evaporated particle transport while a modified surface binding energy (sbe) model is used for sputtered particles emitted at temperatures higher than the melting point of Li.

The liquid Li surface-response model used here is improved from the model used in the earlier Brooks *et al* paper on NSTX-LLD modelling [5]. The model used in that initial work was based on a simple *ad hoc* temperature-dependent binding energy in TRIM-SP [12] calibrated for low-energy He irradiation. TRIM-SP was modified with additional 'soft' collisions in that model to simulate changes of the energy loss term at the surface absent in the BCA-based technique. However, the term corresponding to many-body interactions (also prevalent in ion-induced liquid Li surface response) leading to a change in the particle's momentum (or direction)

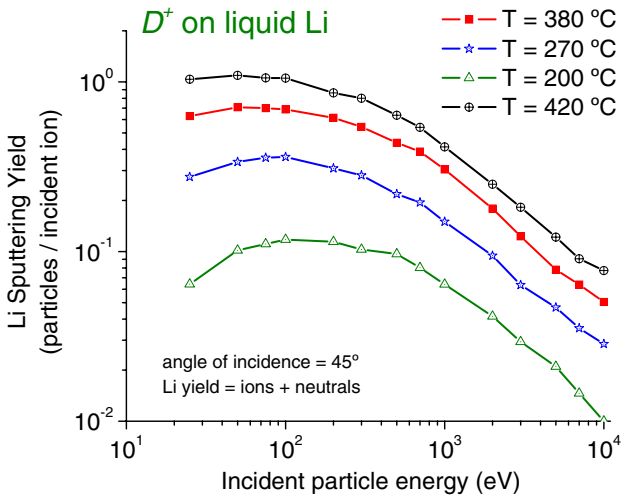

Figure 3. Binary collision approximation TRIM-SP with temperature-dependent model of the sputter yield of lithium at various system temperatures by D^+ ions at 45° incidence. These yields are for total lithium emission (atoms + ions) into free-space.

was absent in that work. Two important mechanisms are included in the new surface-response model derived from MD-TRIM included in this paper and shown in figures 2 and 3. One is the many-body nature of the near-surface collision cascade characterized by the energy and angular recoil distribution presented by Allain *et al* [10] and second, the relative binding of the emitted particle with neighbouring surface atoms before emission (so-called minimum escape energy). For example, in the former mechanism, self-consistent MD-TRIM results show that at higher liquid-metal temperatures a larger amount of the incident energy is transferred to primary knock-on atoms (PKAs). The many-body near-surface model included in this work is critical not only for physical sputtering but also for the other surface-response mechanisms addressed here: Li ion reflection, Li evaporation and sputtered Li charge state. This is because many-body interactions can affect both the near-surface recoil distribution and thus the sputtered and low-energy reflected particle energy distributions. Figure 3 shows the sputter yield of liquid Li by D bombardment for various surface temperatures using the semi-empirical model with TRIM-SP. The model covers the range of incident D^+ particle energies from 25–10 keV at 45° incidence. The model agrees well with the experimental data on D-treated liquid Li sputtering. For example, for a temperature ($T = 280$ °C) and incident particle D^+ energy of 700 eV the sputter yield is 0.2 ± 0.035.

3.2. Trace carbon mixing with liquid lithium

To simulate erosion/recycling of carbon at the liquid lithium surface of the LLD, DYNAMIX (DYNamic transport of multi-Atom material MIXing) runs are conducted that account for particle mixing and fluence dependence of the partial sputter yield of C and Li atoms [13]. Depth profiles of the implanted C atoms in lithium are simulated with DYNAMIX as a function of fluence and subsequent carbon and lithium sputter yields from D sputtering. Simulations account for mixed beam incident on a lithium surface (assumed to be at room temperature) based on REDEP/WBC calculations (at/near the strike point) that give the incident carbon and deuterium ion energies. For this case, a mixed beam having carbon in three charge states, C^+, C^{2+}, C^{3+} and D^+ at 1628 eV, 2378 eV, 3128 eV and 920 eV, respectively (assuming pre-sheath thermalized carbon content, and sheath-acquired energy, for strike-point plasma conditions). The beam contains 2% carbon (typical NSTX core-plasma content) and 98% deuterium. The simulation is carried out for a fluence of 10^{21} m^{-2}. Simulations are conducted for both normal incidence and 45° incidence, each case with 10^6 histories. The target is simulated with a sbe weighted by concentration of top monolayer surface atoms between C and Li. The sbe at room temperature for Li is 1.67 eV, for carbon, 7.4 eV. The relative concentration at the top monolayer is >99% Li atoms. For higher temperatures, the new thermal sbe model (as shown in figure 2) discussed above is used, and for example at 350 °C the 0.46 eV sbe is used for Li surface atoms. At this time there is no model for what the binding would be for C surface atoms in lithium at higher temperatures. However, it is known the effective sputtering of Li–C measured for total particles sputtered of Li and C atoms induced by low-energy He irradiation [14] is significantly reduced compared with either erosion between Li or C surfaces bombarded by He ions. For example, at 200 eV He^+ at 45° incidence the sputter yield is about 0.02 ± 0.008 atoms/ion. This erosion level would be equivalent to a 400 eV D^+ particle. The mechanism for erosion reduction is still under investigation; however, it is conjectured that Li–C form very strong and stable ionic-covalent bonding that significantly reduces the *total* sputter yield from these surfaces. It should be noted that similar reduction of erosion yield is found for Li coatings on boron/carbon coatings in the TJ-II machine in Spain [4]. Allain *et al* also measured that over 95% of the sputtered plume from D and He irradiation-induced bombardment of lithiated graphite consisted of Li atoms and this result was corroborated independently by Racic *et al* [15, 16].

The results of lithiated graphite coating erosion consisted of thin Li coatings on graphite surfaces where the concentration of carbon was much greater than would be reached by assuming a 2% C impurity in the D plasma; therefore, we conjecture that the sputtered plume would be dominated by Li atoms for the C/Li mixing NSTX scenario on the LLD. We note, however, that these results do not take into account any strong ionic or covalent bonding that may take place between C and Li atoms at the surface of the LLD, which could in principle lead to major changes in surface erosion and surface chemistry with implications to D retention as shown by Taylor and Nieto-Perez *et al* [17, 18]. Furthermore, charge-transfer mechanisms, as discussed in the next section, cannot be modelled for the Li–C system given the complexity of the electronic properties of carbon [19]. The strong Li intercalation in graphite, even at temperatures of 100 K [20], also complicates matters in that the intercalation to graphitic basal planes alters the electronic states of both Li and C atoms. Future work will address this pressing issue.

3.3. Charge state of evaporated and sputtered lithium

The charge state of emitted particles for alkali metals involves the mechanism of resonant charge transfer at the surface [21]. Since alkali metals have a large energy gap between their

first and second ionization potentials, most of the emitted Li particles are singly ionized. Emission as an atom or ion then depends on whether the ion survives surface neutralization (and in the absence of any other free electrons other than conduction electrons of the metal—which we assume here to be the case for lithium). This survival depends on surface transit time and hence energy/velocity. Two mechanisms of ionization/neutralization occur for surfaces exposed to plasma in a fusion device. However, they are distinctly different in both time and spatial scale. One mechanism involves the emission of a target particle from the condensed phase (e.g. solid, liquid) to vacuum. The particle can initially emit as an ion and in the time scale of about 10^{-15}–10^{-12} s be readily neutralized in the first 0.2–0.4 nm from the surface plane. The second mechanism involves these emitted neutrals and, in the order of about 10^{-6}–10^{-4} s, become ionized by electrons in the edge plasma over fractions to a few millimetres. These ions are then re-directed to the surface due to the plasma sheath.

For *evaporated* particles with a near thermal distribution, the order of 0.1 eV energy is small compared with sputtered energies (∼1–100 eV), and most of the evaporated plume will be neutralized in the surface. (See figure 2 which uses this model to predict the ionizing probability from room-temperature particles to high-energy particles.) So for ∼0.1 eV, we estimate the ionization probability as about 10%, which we simplify to zero, for the REDEP/WBC analysis. (The REDEP/WBC analysis treats the separate process of near-surface, *plasma* ionization of emitted atoms, and to be discussed, this is high for evaporated Li). The model above is only zeroth order since the conduction-electrons-only assumption and resonance charge-transfer models generally depend on quantum mechanical mechanisms that are the subject of fundamental research. These mechanisms include the resonant nature of electronic transitions between the emitted charged particle and the modification of electronic states of surface atoms. Furthermore, liquid–metal stratification in surface atoms (a known phenomenon in liquid-metal surfaces) has implications on the probability of neutralization discussed above primarily due to possible effects on the sputtered particle energy distributions [22, 23]. Since the ion emission probability is sensitive to both the emission velocity as well as the position of the emitted particle from the surface, topology can also have an important effect. Treatment of realistic corrugated surfaces and their implications on neutralization probabilities is the subject of on-going research beyond the scope of this work [24]. For *sputtered* lithium the model used in our previous studies used a fixed model that 2/3 of sputtered material is singly ionized lithium. This remains consistent; however, we now update this model with temperature-dependent data of the secondary sputtered ion fraction based on previous work by Allain *et al* [8].

3.4. Lithium ion reflection at surface

As discussed in [5, 21] sputtered Li^+ ions are essentially reflected instantaneously by the sheath electric field and return to the surface, with energy equal to their sputtered energy. Subsequently they stick or reflect from the surface. We reassessed these effects and found surface-response models included in our previous work were adequate for this work [5]. Ultra low-energy (also known as a 'hyperthermal' energy region) incident Li^+ particles were modelled using atomistic simulations and the reflected ion probability used a similar model for sputtered Li ions, as shown in figure 2. The model also included reflection as a function of surface temperature between 200 and 380 °C. For hyperthermal energies typical of the *sputtered* energies (e.g. 1–10 eV), governed mostly by the Thompson distribution, the reflection coefficient of sheath-reversed Li^+ ions varied between 0.02 and 0.10 for temperatures between 200 °C and 380 °C, respectively. The fraction of those particles *reflected as ions* did not vary strongly with temperature but rather with emission energy. A lower emission energy range 0.1–4.0 eV resulted in about 50% reflected ions per incident redeposited Li ion. The net effect is an effective atom sputter coefficient, $Y_o^{\text{eff}} = 0.443$ at 380 °C, where Y_o^{eff} is defined as the ratio of total emitted (sputtered plus reflected) lithium atom flux to incident deuterium ion flux. Similar to the charge-exchange models for sputtered particles *scattered or reflected* particles also have strong sensitivity to the emitted velocity of the particles and surface conditions [24]. Therefore, the reflected ions discussed here do not account for Li/C mixing due to lack of data on the ion-induced reflection and ion fraction coefficients.

3.5. Lithium on porous metallic substrates

The NSTX LLD will consist of a static Li thin film deposited on a porous Mo substrate and this has implications for the above discussed mechanisms. Recent experimental work by one of us (Allain) with 1–5 μm deposited thin films of Li at temperatures above 200 °C showed evidence of Li–Mo mixing and mobility in the 100–200 μm porous Mo structure. Mo oxides were also shown to play a role on lithium surface chemistry at temperatures between 200 and 550 °C. In addition, evaporation of thin lithium films was found to be 1–2 orders of magnitude *lower* than those predicted by vapour pressure of pure lithium. Implications of lithium percolation and diffusion in the LLD porous Mo substrate will be addressed in a future publication [25]. For this work we assume that lithium fill is sufficient to assume a pure liquid Li surface layer.

4. REDEP/WBC analysis of LLD sputtering/evaporation

Using the above sputter yields, velocity distributions, sputtered charge state and surface reflection models, we use the REDEP/WBC code package to compute lithium sputtering and evaporation from the LLD surface and subsequent impurity transport in a volume ∼12 cm wide radially by full coverage toroidally, with poloidal dimension extending from 0 to about 20 cm perpendicular to the divertor surface ('Z'-direction), according to figure 1 UEDGE computational grid. Briefly, the WBC Monte Carlo code computes the transport of surface emitted impurity atoms and ions in a background plasma, using full 3D, full-kinetic treatment, including sub-gyroorbit motion and detailed charge-changing and velocity-changing collisions with the plasma ions and electrons. Input plasma parameters are from a typical UEDGE 2D 'low-recycle' solution, with 0.65 D^+ on Li 'reflection' coefficient (35% D^+ retention), and 2 MW heating power (OH and RF) with 1.8 MW power flow from

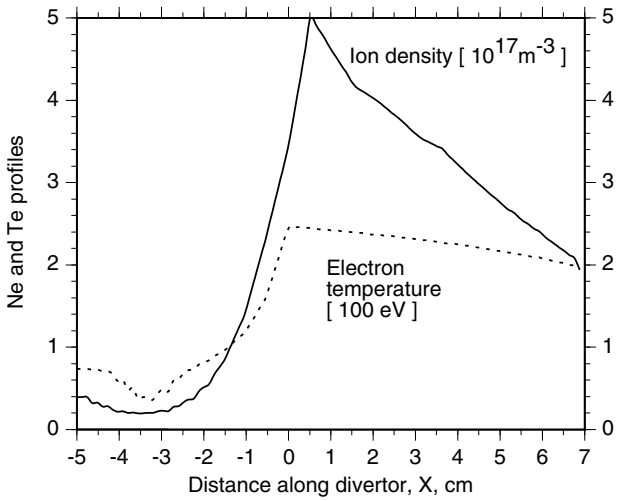

Figure 4. Plasma solution at the LLD, for $R = 0.65$ recycle parameter. From [26].

the core boundary [26]. This plasma solution also includes the LLD surface temperature profile, at shot flattop end time 2.01 s (maximum 281 °C). Relevant plasma parameters here are the electron and ion densities and temperatures, plasma flow speed, and magnetic and electric fields.

Although the binding energy of Li varies with surface temperature, we use a reasonably accurate fixed binding energy of 0.46 eV for the reference calculations, such binding energy being characteristic of the peak temperature. (We studied the sensitivity to binding energy and did not find significant qualitative differences, in particular our conclusions are not significantly changed for a non-elevated temperature Li binding energy of 1.67 eV).

Figure 4 shows UEDGE solution plasma density and electron temperature profiles at the LLD surface. The WBC computation is made on a full 3D grid-free space, using interpolation to compute the plasma parameters at an arbitrary point. The UEDGE peak ion temperature, T_i, at the plate (not shown) is about 1/3 of T_e; and both temperature and density are fairly constant along poloidal field lines although there is some variation. Compared with the previous NSTX plasma solution studied [5] the electron temperature is higher (peak ∼244 versus 185 eV) and density is much lower (factor of ∼5); thus lithium collisionality with the background deuterium plasma will be much less (factor of ∼5 less for Li atom electron-impact ionization and ∼8 less for Li ion velocity-changing collisions with the plasma ions and electrons).

The analysis uses Li I density-dependent and T_e-dependent electron-impact ionization rate coefficients from ADAS [27]. T_e-dependent rates used for Li II–Li IV from previous supplied ADAS data (very little higher-state ionization takes place, in this low-recycle/low-density regime).

For the reference analysis incident particles on the LLD are D^+ ions from the incoming plasma and redeposited lithium ions. The incident D^+ flux is determined by the position-dependent plasma fluid speed at the divertor, density and the net magnetic field angle with the divertor surface. (D^0 charge-exchange sputtering information is not available but would not have a major effect on sputtering, due to lower fluxes than D^+ ions, and at lower energies). As per the above discussion of Li surface conditions, we also analyse a case with a 2% incident carbon ion content, estimated [26] based on present data and LLD simulations, as being due to charge-exchange sputtering of the NSTX first wall and LLD surrounding carbon areas.

In order to determine the appropriate sheath model for the WBC analysis, the BPHI-3D sheath code [29] was run for the NSTX-LLD (strike point) plasma parameters and magnetic field. This code solves for self-consistent sheath parameters for highly oblique magnetic field geometries, with full plasma ion trajectory computation, and assuming the Boltzmann electron model. The usual dual structure (Debye sheath + magnetic sheath) is found *not* to be present, due to the weaker magnetic field, and less oblique B-field incidence, namely 0.5 T and 5°–10° (from surface), respectively, in NSTX, versus 1°–2° incidence and >3 T field for most major tokamaks, e.g. ITER, CMOD, DIII-D. The BPHI-3D result of a Debye-sheath-only is therefore used here for NSTX calculations. This differs from our previous analysis [5]. The locally varying sheath potential model, however, remains unchanged at $e\phi = 3kT_e$. (We note, also, that the sputtered lithium ion flux is too low to significantly affect the sheath, for non-runaway conditions). One effect of the Debye-only sheath is that the average incident angle of D^+ is about 25° from normal, which is less oblique than for a dual-structure sheath. However, we use 45° average sputter D^+ yields here as a conservative (higher sputtering) case.

5. Results

5.1. Reference case-sputtering

For the reference case of D and Li incident on a pure liquid lithium surface, the results are encouraging, showing moderate lithium sputtering and low potential for core-plasma Li contamination. Figure 5 shows typical computed trajectories for sputtered Li transport. Table 1 summarizes transport parameters of this and other cases.

There are several interesting physics observations: (1) the mean free path for lithium atom electron-impact ionization is large, of order 10 cm, for the NSTX low-recycle plasma regime studied, (2) the Li^{1+} ion gyroradius is large (∼5 mm), (3) as mentioned, there is low Li ion collisionality with the background plasma. Due to these points we note that a kinetic, sub-gyro orbit analysis is clearly required, e.g. as is done here via WBC.

The sputtered Li current is 1.43×10^{20} s^{-1}. Most is from D^+ sputtering with 10% from self-sputtering. A total of 59% of the sputtered lithium is ionized within the LLD computation zone, and 94% of this ionized material is redeposited on the LLD; therefore, with 45% of sputtered material escaping the zone—mostly as atoms. The D^+ current to the LLD is 1.99×10^{21} s^{-1}. The ratio of sputtered Li current to incoming D^+ current is thus 7.2%. The lithium ion density is shown in figure 6. The lithium to deuterium ion density ratio in the near-surface LLD region is of this same order of 7%; a moderate value which will not have a major effect on the plasma solution. About 10% of sputtered lithium reaches the WBC near-surface zone/core-plasma boundary ($Z \sim 20$ cm) thus being potentially able to enter the core plasma. We roughly estimate the maximum potential core concentration (Li/D) as

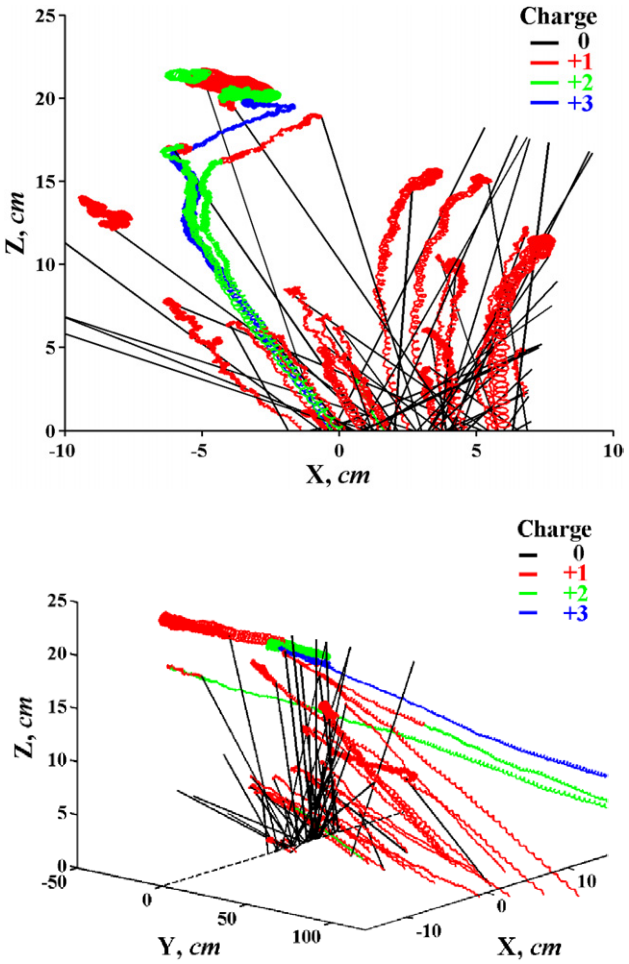

Figure 5. Fifty typical sputtered lithium trajectories, (*a*) 2D view, (*b*) 3D view. ('*X*' = XWBC, '*Z*' = ZWBC, as defined in figure 1, '*Y*' is the toroidal direction). Li atoms launched initially along $y = 0$, per D^+ impingement, and from general locations from self-sputtering by redeposited ions; trajectories terminate if leaving NSTX computational volume; some ion trajectories here computed for full toroidal extent but not fully shown.

1%, using the transport parameters here and with assumptions of equal D and Li core-plasma transport/confinement times, such an estimate rationale was discussed in Brooks *et al* [28]. (A detailed analysis would further track sputtered Li transport in the full UEDGE region, but this is not critical here due to the low contamination potential we deduce from WBC).

Also, although WBC volume escaping particles are not tracked further, we can estimate that 36% of the sputtered Li, or $5.2 \times 10^{19}\,s^{-1}$, would impinge on the various (non-LLD) carbon surfaces. The ratio of this deposited lithium current to the D^+ current to LLD is ~3%; thus representing some additional D-pumping capacity, but not much.

Figure 7 shows the gross and net LLD erosion rate profiles. The peak gross erosion rate is $\sim 10\,nm\,s^{-1}$, with peak net rate of $\sim 5\,nm\,s^{-1}$. Thus, a 2 s shot would involve a peak loss of ~10 nm of the Li surface.

5.2. Higher surface temperature cases

To assess the sensitivity of lithium sputtering to surface temperature we ran cases with the LLD surface temperature increased by a fixed amount at each point. (These runs include the effect of binding energy decrease at higher temperature). These cases could represent longer discharge times and/or higher initial temperature. However, they would only roughly describe higher power cases since the plasma parameters would change for such higher power. We describe results in terms of the peak surface temperature: for 350 °C peak temperature (increase of 69°), the sputtered Li current increases by 67% (over the reference), with a 16% self-sputtering fraction; the peak net erosion rate is $11.6\,nm\,s^{-1}$. For 400 °C, the sputtered Li current increases by 500%, with a 35% self-sputtering fraction; the peak net erosion rate is $30\,nm\,s^{-1}$. Finally, for 450 °C, runaway self-sputtering occurs. Thus, 350 °C peak temperature or below appears acceptable, 400 °C is questionable (~35% ratio of sputtered Li to incoming D) and ~450 °C or above is not acceptable. Of course, these limits are model dependent.

5.3. Lithium evaporation

For the reference surface temperature profile the Li evaporation rate is negligible, at $\sim 1 \times 10^{17}\,s^{-1}$, or 3 orders of magnitude less than the sputtered current. To assess the effect of higher temperatures we made a computer run launching Li atoms from a 2.5 cm wide region centred at the LLD strike point, and with thermal atom emission energy spectrum—this to generically determine the fate of evaporated material at any temperature.

According to table 1 results, 82% of evaporated lithium is redeposited, giving a net loss rate of 18% of the gross rate. The high redeposition rate is due to thermal lithium atom ionization within about 2 cm from the surface, and subsequent strong redeposition due to collisional friction with the incoming D^+ plasma. Therefore, the acceptable evaporation rate—as set, for example, by core-plasma lithium contamination—would be roughly five times higher than the rate not considering redeposition. Another positive result is that ionization of evaporated lithium atoms occurs almost completely outside of the LLD (Debye-only) sheath, which would appear to eliminate a sheath collapse limitation on surface temperature [29]. While helpful, however, the significance of the above points is limited by the exponential increase in vapour pressure with surface temperature, i.e. even a factor of five increase in acceptable evaporation rate does not gain that much temperature margin. Still, the strong redeposition of evaporated material will provide some temperature margin for LLD operation.

5.4. Carbon sputtering of lithium and carbon transport

For the case of 2% carbon impinging on LLD we compute, using TRIM-SP sputter yields for C on Li, an increase in Li sputtering of about 10% from the reference case, thus not significantly affecting lithium erosion/transport. In terms of sputtering of a carbon layer itself on LLD, we ran WBC launching C atoms with the binding energy/distribution of C at room surface temperature (i.e. 7.4 eV). We note that at normal incidence of the mixed D–C beam, the maximum depth concentration of C atoms totals 1.5% at a depth of 15 nm. At 45° incidence, the maximum depth concentration of C atoms peaks at about 1.4% and a depth of about 5–7 nm for a total fluence of $10^{21}\,m^{-2}$. As shown in table 1, the predicted transport of sputtered C from the LLD is roughly similar to

Table 1. WBC NSTX-LLD analysis: transport summary for three emitted materials (100 000 histories/simulation).

Parameter	Sputtered lithium[a]	Evaporated lithium[b]	Sputtered carbon[c]
Emitted atom energy distribution	Modified Thompson, per TRIM-SP; sbe = 0.46 eV	Thermal, with 0.1 eV average energy	Modified Thompson, per TRIM-SP; sbe = 7.4 eV
Mean free path[d] (cm)	6.4	2.1	8.1
Transit time[e] (μs)	36	15	50
Charge state[e]	1.06	1.01	1.6
Incidence (elevation) angle[e] (°) from normal	19	12	22
Energy[e] (eV)	406	342	658
LLD redeposition fraction	0.553	0.822	0.419
Fraction to outer region	0.225	0.086	0.243
Fraction to inner region	0.132	0.089	0.185
Fraction to near-surface/ core-plasma boundary[f]	0.090	0.003	0.147

[a] From ∼12 cm wide LLD surface.
[b] From LLD central 2.5 cm region.
[c] From re-sputtering of wall-to-core plasma-to-LLD deposited carbon.
[d] Normal-to-surface; for LLD region ionized material.
[e] Average for LLD redeposited ions on divertor.
[f] At ∼20 cm from the LLD surface and within the UEDGE grid.

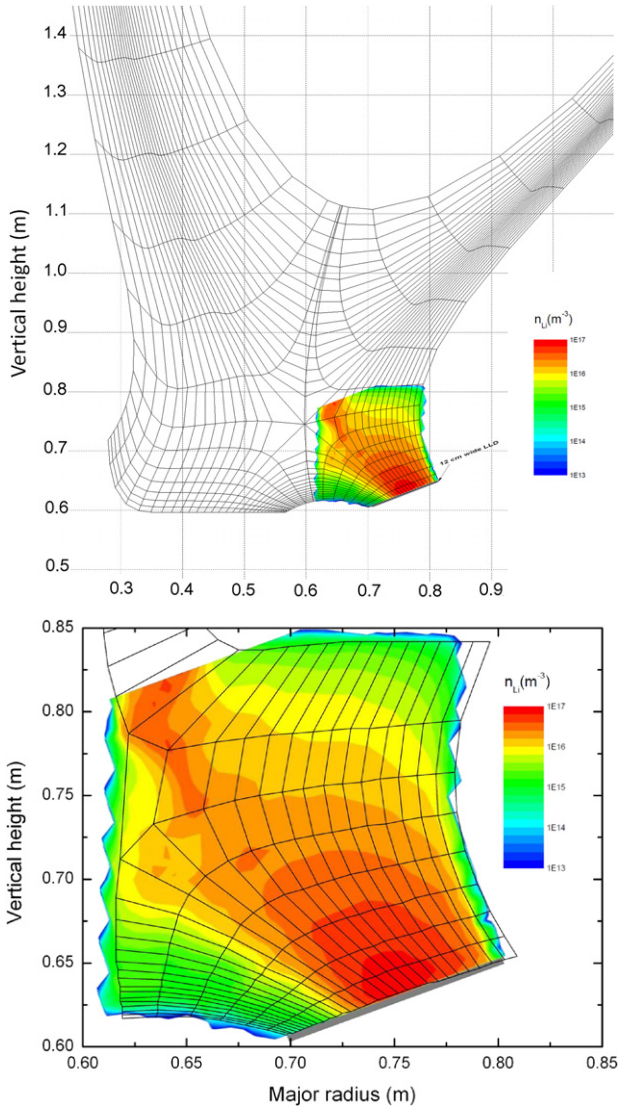

Figure 6. REDEP/WBC computed lithium ion density, shown on UEDGE grid, for reference case plasma solution.

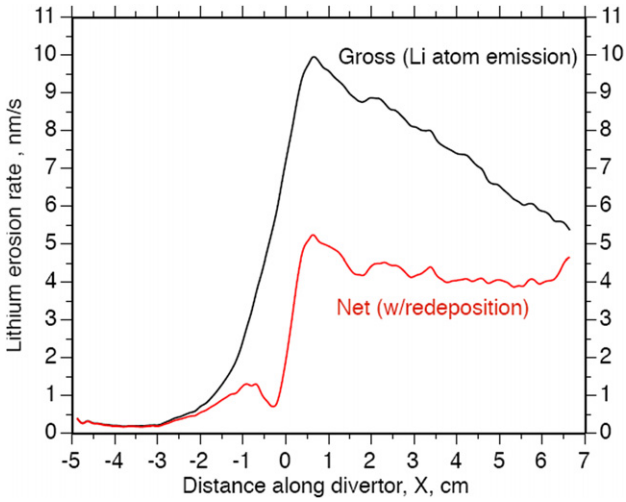

Figure 7. Gross and net lithium erosion rate along NSTX LLD; for reference case plasma solution.

sputtered Li. In general, it appears that the influence of carbon is negligible for the conditions studied, and assuming that surface ion mixing is the only mechanism that contributes to any changes in liquid Li surface performance with incident carbon mixing.

6. Discussion

The surface-response models used here ignore any effect of surface morphology on surface properties. For liquid lithium the mechanisms that can vary the surface morphology include surface oxidation (formation of Li oxide islands and micro- to macroscopic slag), MHD induced surface fluctuations, TE MHD induced surface fluctuations, synergistic ion-induced enhanced erosion and thermal-effective mechanisms that may enhance or reduce evaporation. The assumptions made using TRIM-SP and DYNAMIX surface-response codes are valid from the standpoint that liquid lithium can be considered

amorphous and incident particle energies are large (typically >100 eV) in low-recycling regimes. One particular challenge for the LLD on NSTX is the fact that the liquid is static. This can lead to limitation on retention of hydrogen due to possible oxide formation on the static liquid Li surface. This effect is difficult to simulate due to the environment-dependent surface chemistry conditions. Since retention and recombination occur at the first few tens of nanometres, it is unlikely that thin versus thick coverages of liquid lithium would affect hydrogen retention. Morphology-induced changes due to small impurities such as carbon on the liquid Li surface is yet another topic for further investigation.

7. Conclusions

Liquid lithium divertor evaporation, sputtering and transport have been modelled for NSTX, for typical anticipated high power plasma shots, using updated coupled surface models, and plasma edge and impurity emission/transport codes. The goal was to determine the basic compatibility of the LLD with NSTX higher power operation, from the standpoint of Li evaporation and sputter erosion, and core-plasma contamination (but not including MHD or plasma transient effects). The results are encouraging showing significant D^+ sputtering but non-runaway self-sputtering, acceptable net erosion, and acceptable core-plasma contamination potential, of order 1%. There also appears to be about a 70–100 °C margin in surface temperature, presumably equating to higher heat flux capability.

As discussed, however, liquid lithium is a very complex material, involving, e.g., sputtered charge states, surface chemistry/mixing/trapping with D, C and redeposited Li, and related issues. One particular challenge will be how to predict D retention and recycling of the LLD for a lithium surface that is evolving with surface impurities and 'slag' during the course of NSTX shot operation. Modelling, experiments and code/data validation work with plasma interactions on liquid lithium surfaces thus clearly need continuation.

Acknowledgments

We thank graduate student R. Ochoukov (MIT) for help with the BPH-3D sheath code calculation for NSTX and Purdue students Guojing Hou and Eric Yang for DYNAMIX calculations. This work is supported in part by the US DOE Contracts DE-FG02-08ER54990 and DE-AC02-09CH11466.

References

[1] Majeski R. *et al* 2006 *Phys. Rev. Lett.* **97** 075002
[2] Kugel H.W. *et al* 2008 *Phys. Plasmas* **15** 056118
[3] Mirnov S.V. *et al* 2006 *Plasma Phys. Control. Fusion* **48** 821
[4] Tabarés F.L. *et al* 2010 *Contrib. Plasma Phys.* **50** 610
[5] Brooks J.N., Allain J.P., Rognlien T.D. and Maingi R. 2005 *J. Nucl. Mater.* **337–339** 1053
[6] Stotler D.P. *et al* 2010 *Contrib. Plasma Phys.* **50** 368–73
[7] Brooks J.N. 2002 *Fusion Eng. Des.* **60** 515
[8] Allain J.P., Coventry M.D. and Ruzic D.N. 2007 *Phys. Rev.* B **76** 205434
[9] Doerner R.P., Baldwin M.J., Krasheninnikov S.I. and Whyte D.G. 2003 *J. Nucl. Mater.* **313–316** 385
[10] Allain J.P., Ruzic D.N., Coventry M.D., Alman D.A. and Nieto M. 2005 *Nucl. Instrum. Methods Phys. Res.* B **239** 347
[11] Qiu H.-T. and Ruzic D.N. 2005 *J. Nucl. Mater.* **337–339** 1029
[12] Allain J.P., Coventry M.D.and Ruzic D.N. 2003 *J. Nucl. Mater.* **313–316** 641
[13] Hou G. 2010 The development of a dynamic radiation-surface interaction simulation code *MSc Thesis*
[14] Allain J.P. *et al* 2009 *J. Nucl. Mater.* **390–391** 942
[15] Racic M. *et al* 2009 *J. Nucl. Mater.* **390–391** 1043
[16] Ibano K. *et al* 2010 *IEEE Trans. Plasma Sci.* **38** 341
[17] Taylor C.N. *et al* 2011 Surface chemistry and physics of deuterium-retention in lithiated graphite *J. Nucl. Mater.* at press
[18] Nieto-Perez M., Allain J.P., Heim B. and Taylor C.N. 2011 Chemical and physical erosion of carbon and metallic substrates containing lithium during low-energy deuterium ion irradiation at press
[19] Caragiu M. and Finberg S. 2005 *J. Phys. Conden. Matter* **17** R995
[20] Johnson M.T. *et al* 1986 *Surf. Sci.* **178** 290
[21] Allain J.P., Brooks J.N., Alman D.A. and Gonzalez L.E. 2005 *J. Nucl. Mater.* **337–339** 94
[22] Pershan P. 1996 *Physica* A **231** 111
[23] Rice S.A. 1996 *J. Non-Cryst. Solids* **205–207** 755
[24] Wayne Rabalais J. 2003 *Principles and Applications of Ion Scattering Spectroscopy* (Hoboken, NJ: Wiley)
[25] Taylor C., Heim B. and Allain J.P. 2011 *J. Appl. Phys.* at press
[26] Stotler D.P. 2009, PPPL, personal communication
[27] Loch S.D. *et al* 2006 *At. Data Nucl. Data Tables* **92** 813
[28] Brooks J.N., Allain J.P. and Rognlien T.D. 2006 *Phys. Plasmas* **13** 122502
[29] Brooks J.N. and Naujoks D. 2000 *Phys. Plasmas* **7** 2565